academicJournals

Vol. 16(25), pp. 1366-1378, 21 June, 2017
DOI: 10.5897/AJB2017.16021
Article Number: 6383CB064862
ISSN 1684-5315
Copyright © 2017
Author(s) retain the copyright of this article
http://www.academicjournals.org/AJB

African Journal of Biotechnology

Full Length Research Paper

Kinetic characterization and molecular modeling of trehalose-6-phosphate phosphatase from *Anopheles gambiae* and expressed in *Pichia pastoris*

Marcos Cézar Fernandes Pessoa[1], Érika Izumi[2], Sandra Patrícia Zanotto[1] and Spartaco Astolfi-Filho[1]*

[1]Laboratory of DNA Technology, Biotechnology Department, Multidisciplinary Support Center, Federal University of Amazonas, Manaus, Amazonas, Brazil.
[2]Federal University of Technology, Curitiba, Paraná, Brazil.

Received 4 April, 2017; Accepted 14 June, 2017

Trehalose-6-phosphate phosphatase (TPP) is one of the primary enzymes involved in the synthesis of trehalose, the main sugar found in insect hemolymph. In the present study, we report for the first time heterologous expression in *Pichia pastoris*, characterization and homology modeling of TPP from *Anopheles gambiae* mosquito. Purified TPP recombinant exhibited a molecular weight of approximately 36 kDa with optimum pH of 8.0, optimum temperature of 38°C, and the K_M was 3.19 ± 0.10 mM. Inhibition tests revealed that $CaCl_2$ and $Ca(NO_3)_2$ at 5 and 25 mM, respectively, were effective inhibitors of TPP activity. Homology studies and molecular modeling indicated high similarity of the TPP tridimensional structure with TPP enzymes deposited at a data bank and these homology studies confirmed that it is a trehalose phosphatase with conserved motifs of the superfamily haloacid dehydrogenase. These results may provide support for the discovering of TPP inhibitors to be used for development of insecticides to control mosquito vectors.

Key words: Trehalose, trehalose-6-phosphate phosphatase, expression, enzyme characterization, homology modeling.

INTRODUCTION

Malaria is a potentially serious infectious disease caused by unicellular protozoans of the genus *Plasmodium* species and is transmitted to vertebrate hosts through bites from females of the mosquito *Anopheles* species (Forattini, 2002; WHO, 2016). Human malaria is a parasitic disease with medical, social and economic importance, and it constitutes one of the most important public health problems worldwide. Malaria is endemic in 91 countries, with 212 million estimated cases and 429 000 estimated deaths from malaria globally in 2015 (WHO, 2016). The vast majority of malaria deaths occur in Africa, especially among children (Garcia, 2010), and the mosquito *Anopheles gambiae* Giles, belonging to the subgenus *Cellia*, is the primary human malaria vector.

*Corresponding author. E-mail: spartaco.biotec@gmail.com. Tel: + 55 92 3305 3240.

Author(s) agree that this article remains permanently open access under the terms of the Creative Commons Attribution License 4.0 International License

Resistance in the mosquito vector to at least one of the insecticides used for malaria control has been detected in 60 countries (WHO, 2016). Thus, studies on the metabolism of the insect vector and main enzymes involved in different metabolic pathways are therefore important for collecting data on the insect's physiology, which can be used in the research and design of insect control strategies.

Trehalose is a non-reducing glucose disaccharide and the primary carbohydrate found in insect hemolymph, thus, its metabolism is a potential target for the rational development of insecticides. This disaccharide serves as a circulating energy source that is similar to glucose in vertebrate blood (Klowden, 2013), and it is synthesized in the insect fat body through the combined action of two enzymes, trehalose-6-phosphate synthase (TPS) and trehalose-6-phosphate phosphatase (TPP) (Karthik et al., 2011). These enzymes have been detected in insects and other invertebrate animal classes but not in humans. The regulation of the trehalose metabolic pathway in insects is well known (Thompson, 2003).

The trehalose biosynthetic pathway was first described in *Sacharomyces cerevisiae* (Cabib and Leloir, 1958). At the insect fat body, trehalose-6-phosphate synthase catalyzes the formation of a trehalose α-1, α-1 glycosidic bond by the condensation of glucose-6-phosphate and glucose from uridine diphosphate glucose, forming trehalose-6-phosphate (T6P). The second reaction is catalyzed by TPP and involves the cleavage of phosphate ester bonds and the release of inorganic phosphate and free trehalose to the hemolymph (Eastmond et al., 2002; Matula et al., 1971). TPP (EC 3.1.3.12) is a member of the superfamily haloacid dehalogenase (HAD) (Collet et al., 1998) and exhibits significant sequence homology with several phosphatases, P-type ATPases (Koonin and Tatusov, 1994) and other members of the family (Rao et al., 2006). TPP displays specific activity for substrate T6P, resulting in trehalose formation in the presence of water, which is characteristic of enzymes of the hydrolase family with phosphatase activity (Elbein, 2009; Klutts et al., 2003; Kormish and McGhee, 2005; Rao et al., 2006).

Gene silencing techniques applied do TPS gene from *Aedes aegypti* (Vaidyanathan et al., 2015) and suppression of activity of trehalase from *Nilaparvata lugens* by inhibitors (Tang et al., 2017) have shown that this pathway is fundamental in the maintenance and survival of insects. In the present study, we report on the expression, characterization and homology modeling of TPP from *A. gambiae.* These results can support the development of new approaches that using the TPP as a molecular target to discovery novel insecticides for use in mosquito vectors control.

MATERIALS AND METHODS

TPP synthetic gene design

The nucleotide sequence of the TPP gene structural region was obtained from the *A. gambiae* genome data bank, which is available at the Kyoto Encyclopedia of Genes and Genomes (KEGG) website (www.genome.jp/kegg/). The DNA sequence was flanked with restriction sites for specific recognition by the endonucleases *Eco*RI and *Not*I, which enabled subcloning of the sequence into the expression and secretion vector for *Pichia pastoris*, pPIC9. A sequence coding a six-histidine tail (*his*^{6}*-tag*) was inserted at the 3' end for purification and identify the confirmation of the expressed protein by immunological assays. The nucleotide sequence was chemically synthesized by GenOne (Rio de Janeiro, RJ, Brazil) and cloned into the vector pBSK. The vector containing the synthetic *TPP* gene was named pBSK-T.

The structural sequence of the *TPP* gene optimized for expression in *P. pastoris* was constructed using the bioinformatics tools KEGG, BLAST, ExPasy, UniProt, CBS Prediction Servers, NEBcutter V 2.0 and Clustal; these tools are available at specialized websites. The theoretical properties of the translated recombinant protein of the *TPP* gene were determined using the ExPASy ProtParam Tool (http://web.expasy.org/protparam/) and the NetNGlyc 1.0 Server (http://www.cbs.dtu.dk/services/NetNGlyc/) and NetOGlyc 3.1 Server (http://www.cbs.dtu.dk/services/NetOGlyc-3.1/) bioinformatic tools.

Cloning and expression

To construct the TPP expression and secretion vector for *P. pastoris*, the synthetic *TPP* coding sequence was freed from the pBSK-T cloning vector by double digestion with *Eco*RI and *Not*I according to the enzyme manufacturer's recommendations (New England Biolabs, Ipswich, MA, USA). The fragment was then purified from agarose gel using an Illustra GFX PCR DNA and Gel Band Purification Kit (GE Healthcare, Little Chalfont, UK) and ligated into the *Eco*RI and *Not*I sites of the multiple cloning site of the pPIC9 vector. The recombinant plasmid was named pPIC-TPP and was used in the transformation of *Escherichia coli* DH10B electrocompetent cells. Plasmid DNA extracted from the *E. coli* DH10B host was subjected to restriction analysis to confirm the correct construction of the recombinant plasmid pPIC-TPP.

The plasmid pPIC-TPP was digested with *Bgl*II for 2 h at 37°C to free the expression cassette containing the TPP coding sequence. The digestion product was used to transform the *P. pastoris* GS115 strain via electroporation, and recombinant clones were selected via auxotroph complementation in minimal dextrose (MD) medium without the addition of histidine. Plates were incubated for 72 h at 30°C.

Heterologous protein expression was induced with 25 ml of buffered glycerol-complex medium (BMGY) and incubated at 30°C under constant stirring at 250 rpm for approximately 24 h. The cells were collected following centrifugation at 4000 rpm for 10 min at 4°C and then resuspended in 50 ml of buffered methanol complex medium (BMMY). The promoter AOX1, which modulates the transcription of the heterologous gene inserted into the host genome, was induced by adding 250 µl of methanol (Pro Analyse) to the cell culture every 24 h to a 0.5% final concentration (v/v). *TPP* gene expression was induced for 72 h at 30°C under constant stirring at 180 rpm.

Western blot analysis

The recombinant clone expressing TPP was selected via colony blot immunoassay, which was performed in plates according to the QIAexpressionist manual (QIAGEN, Hilden, DE) for transformant analysis. The expression of recombinant TPP was confirmed through western blot analysis. Following sodium dodecyl sulfate polyacrylamide gel electrophoresis (SDS-PAGE), the protein was transferred to a nitrocellulose membrane through a semi-dry

transfer system (Gravel, 2002) performed with a Trans-Blot® SD Semi-Dry Transf Cell (Bio-Rad, Hercules, CA, USA) for 1 h under the following conditions: 10 volts, 0.13 A, 1 W. Following the transfer, the nitrocellulose membrane containing the immobilized protein was treated with the antibodies and reagents contained in the WesternBreeze® Chromogenic Western Blot Immunodetection Kit (Invitrogen, Carlsbad, CA, USA) according to the manufacturer's instructions.

Enzyme purification

The supernatant containing the recombinant protein was filtered using a retention membrane with 0.45 µm diameter pores. TPP purification was performed using an ÄKTA purifier (GE Healthcare) coupled to a HisTrap™ 1-ml column (GE Healthcare). The column was pre-equilibrated with 2 ml of binding buffer (20 mM NaH_2PO_4•H_2O; 0.5 M NaCl; pH 7.4). The sample was eluted using an elution buffer (20 mM NaH_2PO_4•H_2O; 0.5 M NaCl; pH 7.4) with an imidazole gradient up to 0.5 M. The fractions were collected at room temperature at a flow rate of 1 ml/min, and absorbance was read at 280 nm. The fractions containing the recombinant protein were analyzed via an SDS-PAGE gel (Laemmli, 1970) stained with Coomassie Brilliant Blue according to the methods of Oakley et al. (1980).

Purified recombinant protein was quantified using a Pierce™ BCA Protein Assay kit (Thermo Scientific, Waltham, MA, USA) according to the manufacturer's recommendations. The assay was performed in triplicate using bovine serum albumin (BSA) as the standard.

Enzyme characterization

Enzyme characterization was performed using 200 ng/µl recombinant enzyme and 1 mM T6P. The assay for TPP activity was measured by determining the release of inorganic phosphate from T6P according methodology descripted by Edavana et al. (2004) and Klutts et al. (2003).

pH effect

The pH effect on the enzyme activity was determined at 37°C and 10 min incubation using the following buffers: 2-ethanesulfonic acid (MES) (pH 5.0 to 7.0), Tris-HCl (pH 7.0 to 9.0) and glycine (pH 8.0 to 11.0).

Temperature effect

The optimum temperature was determined by initially incubating the reaction system over a temperature range between 30 and 80°C and then over a temperature range between 30 and 40°C.

Determination of kinetic constants

Enzyme activity was determined according to a modification of the method by Klutts et al. (2003), which used 1 to 8 mM T6P (Sigma-Aldrich, St. Louis, MO, USA), 2 mM $MgCl_2$, 50 mM Tris-HCl buffer and 1 µl of recombinant enzyme. The reaction was performed for 10 min, and the Michaelis-Menten curve and Lineweaver-Burk plot were obtained.

Effect of chemical inhibitors on TPP activity

TPP inhibition was tested using ethylenediaminetetraacetic acid (EDTA), NaF, $CaCl_2$ and $Ca(NO_3)_2$ at concentrations of 5 and 25 mM and final volume of 50 µl. The reaction was performed for 10 min.

Homology modeling of related TPP enzymes

The identity of the TPP sequence was confirmed through an alignment with TPP from other mosquito species using a BLAST search on the UniProtKB website (http://www.uniprot.org/). Sequences for each vector mosquito were saved in FASTA format. A global sequence alignment of TPP from *A. gambiae* with TPP sequences from other species of vector mosquitoes was then performed, and these sequences were compared with the template sequence from *Thermoplasma acidophilum* (PDB ID: 1U02).

The TPP sequences were submitted to the EMBL-EBI server (http://www.ebi.ac.uk/Tools/msa/clustalw2/) for multiple alignment using the software Clustal Omega 1.2.1 (Sievers et al., 2011). The TPP amino acid sequence was then submitted to the Phyre^2 server (http://www.sbg.bio.ic.ac.uk/phyre2/html/page.cgi?id=index) (Kelley and Sternberg, 2009), and its secondary and tertiary structure was predicted and then compared with tridimensional protein structures deposited at the Protein Data Bank. The theoretical tridimensional structure of TPP was based on the template structure from *T. acidophilum* (1U02). The stereochemical quality of the structure was examined using PROCHECK (Laskowski et al., 1993) and subsequently refined using the software ModRefiner (Xu and Zhang, 2011). The protein was visualized using the software PyMOL (DeLano, 2006).

Modeling the TPP-T6P complex

The molecular docking of the substrate to the TPP active site was modeled using AutoDock 4.2.6 (Morris et al., 1998), a Lamarckian genetic algorithm (Solis and Wets, 1981) and the software PyRx 0.8 (Wolf, 2009). The substrate molecule was obtained from the PubChem Compound Database (Bolton et al., 2008) minimized and converted to PDBQT format using PyRx. The grid box that defines the size of the binding pocket was created using the software AutoGrid (Morris et al., 1998). The grid box was centered at coordinates x=20.8224, y=22.0076 and z=16.1604 Å and the spacing between grid points was 0.375 Å. The AutoDock results were visualized using PyRx, and the most favorable ligand-binding pose was selected based on its conformation and binding energy. The selected docking was analyzed using the Discovery Studio 4.0 Visualizer software (Accelrys, 2013), which was also used to identify the number of hydrogen bonds and other enzyme-substrate intermolecular interactions.

Statistical analysis

The enzyme characterization data (mean + standard error [SE]) were analyzed by performing analysis of variance (ANOVA) using the software GraphPad Prism 5.04 for Windows. The inhibition test data were subjected to Bonferroni correction at $p<0.05$. All of the assays were performed in triplicate. The Bonferroni correction is a standard test of the program used for this analysis type.

RESULTS AND DISCUSSION

The enzyme TPP is present in bacteria, fungi, plants and invertebrates but not in mammals. Its catalytic product (trehalose) is used by these organisms as an energy reserve and for protection against environmental

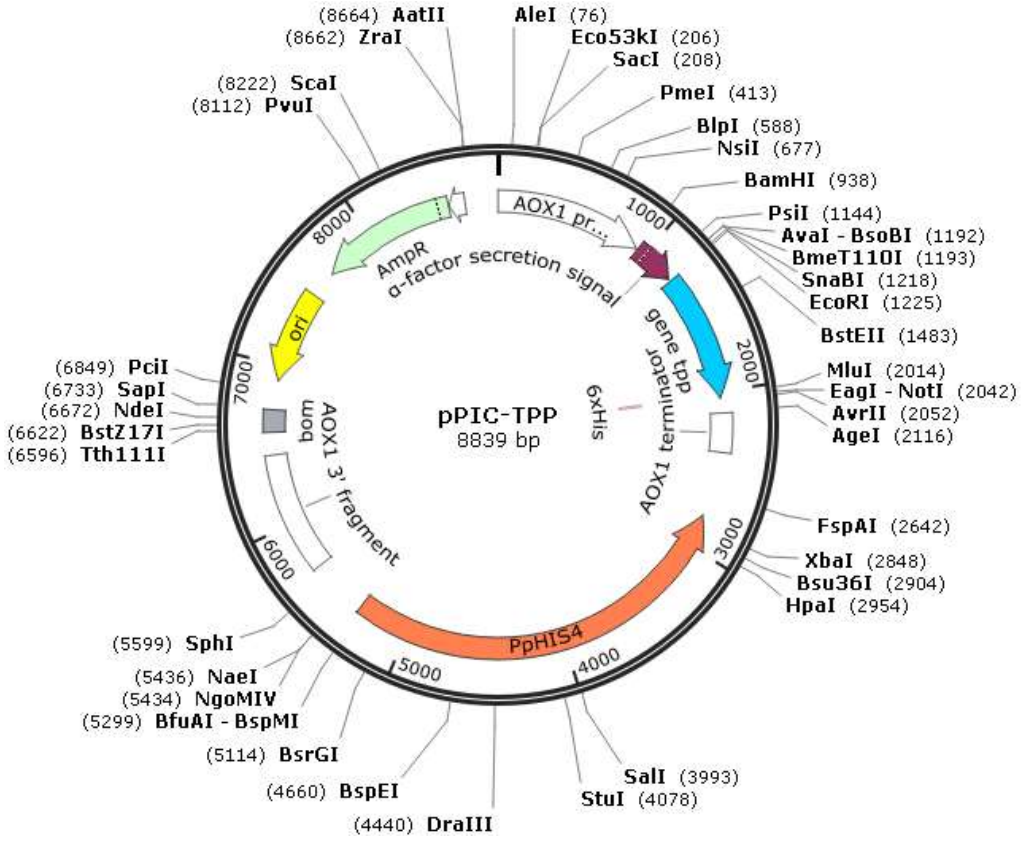

Figure 1. Physical map of the pPIC-TPP recombinant plasmid showing the insertion of the *TPP* gene (in blue) into the vector pPIC9, which is flanked by restriction enzymes *Eco*RI and *Not*I and located after the coding region for the α-factor signal peptide for secretion. The physical map was constructed using the software SnapGene® Viewer 2.4.2.

stresses, such as oxidative and osmotic stress, freezing, desiccation and anhydrobiosis (Behm, 1997; Elbein et al., 2003).

TPP is important for the metabolism and physiology of the mosquito *A. gambiae*, which is an important vector of *Plasmodium falciparum*, the parasite responsible for the most serious form of human malaria in Africa. The nucleotide and amino acid sequences of the *TPP* gene were obtained from the KEGG website and can be found at the following accession: *A. gambiae* (mosquito): AgaP_AGAP008225-PA. The information on this gene available at KEGG are in accordance with the National Center for Biotechnology Information (NCBI) and UniProtKB (Protein Knowledgebase - AgTpp AGAP008225/AgaP_AGAP008225) databases. The *TPP* gene was selected because it codes for a protein that is involved in the formation of disaccharide trehalose in the insect's carbohydrate metabolic pathway. TPP was chosen for cloning and expression because its catalytic product is trehalose, which is not essential for mammal cells, and not glucose, which is the major carbohydrate required for numerous mammalian metabolic pathways (Karthik et al., 2011; Klutts et al., 2003; Kormish and McGhee, 2005; Kushwaha et al., 2011).

After codon optimization and chemical synthesis, the *TPP* gene structural region was cloned into the plasmid vector pPIC9 under control of the AOX *P. pastoris* strong promoter. The physical map of the pPIC-TPP recombinant plasmid resulting from insertion of the *TPP* gene into the expression/secretion vector is presented in Figure 1. The TPP coding sequence is located downstream from the coding sequence for the *S. cerevisiae* α-factor signal peptide, which ensures TPP secretion.

Recombinant clones were obtained through the transformation of *E. coli* DH10B with the ligation product of the *TPP* gene structural region to the vector pPIC9. A transformant clone was selected for subsequent plasmid DNA extraction, and confirmation of the correct construction of the pPIC-TPP recombinant plasmid was performed through restriction analysis. The resulting electrophoresis profile revealed that the freed fragments correspond to the size of the vector pPIC9 (8023 bp) and the *TPP* gene structural region (830 bp), confirming that the structure of the pPIC-TPP recombinant vector was correct (Figure 2A).

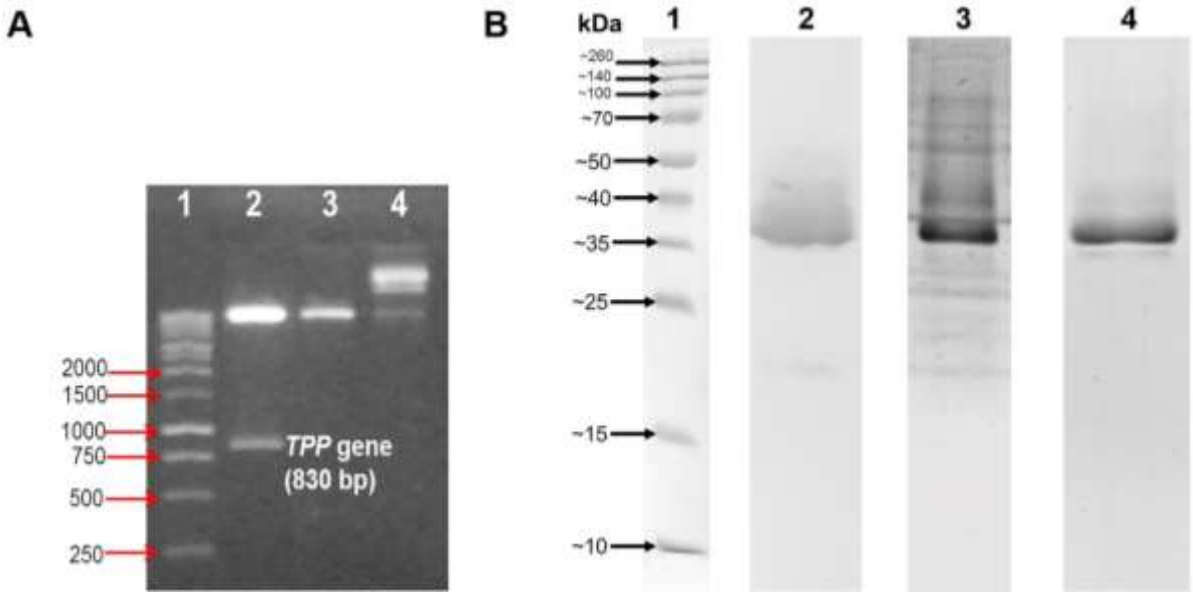

Figure 2. Cloning, expression and purification of TPP from *A. gambiae.* **(A)** Restriction analysis of the pPIC-TPP recombinant plasmid. Lane 1, Marker GeneRuler™ 1 Kb DNA Ladder (Fermentas); lane 2, pPIC-TPP digested with *Eco*RI and *Not*I; lane 3, pPIC9 without insert digested with *Eco*RI and *Not*I; lane 4, pPIC9 not digested. **(B)** Electrophoretic profiles of recombinant TPP. Lane 1, Marker Spectra Multicolor Broad Range Protein Ladder (Thermo Scientific); kDa molecular weights marker varying between 10 and 260 kDa; lane 2, western blotting of recombinant TPP induced for 72 h in BMMY medium; lane 3, electrophoretic profile (15% SDS-PAGE gel) of recombinant TPP; lane 4, electrophoretic profile (15% SDS-PAGE gel) of TPP purified by affinity chromatography.

The expression/secretion of the heterologous protein by a selected clone of *P. pastoris* after incubation for 72 h was analyzed by western blotting of the supernatant using the anti-His^{6}-tag antibody. The results indicated that TPP was efficiently expressed by the *P. pastoris* expression system (Figure 2B, lane 2).

Following confirmation of TPP expression and secretion in the supernatant, recombinant TPP was newly induced. The culture supernatant was analyzed by a 15% SDS-PAGE gel. The TPP recombinant protein was larger than expected for the native protein (Figure 2B, lane 3). In addition, TPP was secreted in large amounts in the supernatant and constituted the largest portion of proteins produced by the yeast, which was observed in the supernatant. A bioinformatics analysis was performed using *ExPASy* and *ProtParam* and estimated a 29.3 kDa molecular weight for non-glycosylated TPP. However, the SDS-PAGE band corresponding to recombinant TPP exhibited electrophoretic migration equivalent to 36 kDa. Because the TPP polypeptide sequence possesses two potential N-glycosylation sites and one O-glycosylation site and because glycosylation affects protein electrophoretic migration in an SDS-PAGE gel, it was inferred that the estimated weight of the recombinant TPP increased from 29.3 kDa to approximately 36 kDa as a result of glycosylation during post-translational processing in the secretory pathway. Recombinant proteins expressed in *P. pastoris* may be larger than expected and exhibit different sizes when analyzed by SDS-PAGE if they are glycosylated (Cregg et al., 2009) or hyperglycosylated (Cereghino and Cregg, 2000).

TPP was purified in one stage using Ni^{2+} resin affinity chromatography and was eluted with 300 mM imidazole upon application of an elution gradient. The purified recombinant protein was analyzed to SDS-PAGE (Figure 2B, lane 4). According to the electrophoretic profile, the recombinant TPP was eluted as a single band that migrated with an apparent 36 kDa molecular weight, which is in accordance with the results presented in Figure 2B.

Following TPP purification, its physicochemical properties were determined. The effects of pH, temperature and inhibitors on TPP activity were determined as well as kinetic constants. To our knowledge, there are no previous characterization studies of TPP from *A. gambiae*.

Recombinant TPP activity was tested in MES-Tris-Glycine buffer in a pH range from 5.0 to 11.0 in 1.0 unit intervals. The recombinant TPP activities at the different pH levels are presented in Figure 3A.

P. pastoris secreted TPP exhibited higher activity between pH 7.0 and 8.0, with a peak at pH 8.0, and it maintained approximately 25% activity at pH 5.0 and 9.0. The optimum TPP pH varies widely among organisms. Among insects, higher activity at pH 7.0 was observed for TPP from the cockroach *Periplaneta Americana* (Friedman

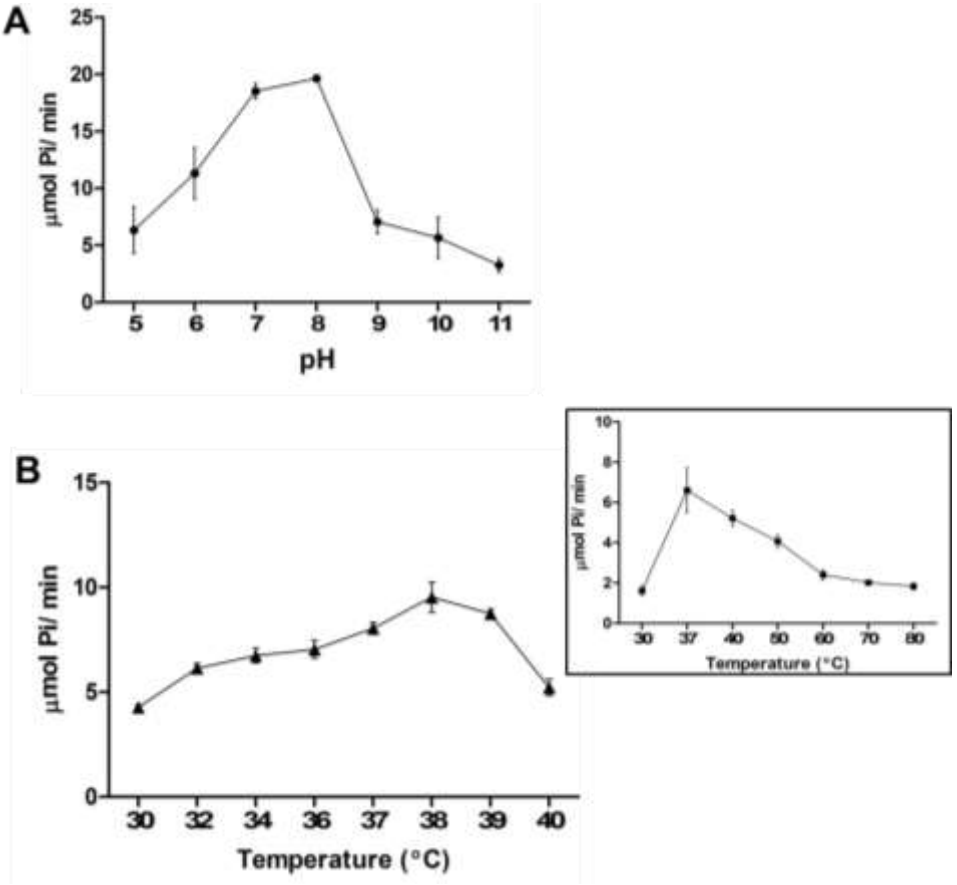

Figure 3. Characterization of recombinant TPP enzymatic parameters. (A) Determination of optimum pH: enzyme activity was measured in MES-Tris-Glycine buffer (50 mM) at different pH (5-11). Optimum pH for *A. gambiae* TPP activity was 8.0. (B) Determination of optimum temperature: enzyme activity was measured at different temperatures, and the enzyme activity over a wide temperature range (30 - 80°C) is presented in the right upper corner, with activity peak at 37°C. The optimum temperature over a narrow temperature range (30 - 40°C) is highlighted. Based on this range, the TPP optimum temperature, at which it exhibits maximum activity, was 38°C.

and Hsueh, 1979). TPP from the black blow fly (*Phormia regina*) also exhibited the highest activity at pH 7 and maintained activity between pH 6.0 and 8.5 (Friedman, 1966). Therefore, the optimum TPP pH does not present large variations among different classes of insects.

Regarding the temperature effect, purified TPP was first evaluated at a temperature range between 30 and 80°C in Tris-HCl buffer at pH 8.0 (Figure 3B, right upper corner), and its catalytic action was then evaluated at a narrower temperature range, between 30 and 40°C (Figure 3B, highlighted). Recombinant TPP exhibited a maximum activity of 9.53 µmol Pi/min at 38°C (Figure 3B). This temperature was therefore considered the optimum temperature for the activity of TPP from *A. gambiae*.

Friedman (1966) studied *P. regina* and reported that the highest TPP activity was at 46°C and that 85% activity was maintained at 57°C for 15 min. Friedman and Hsueh (1979) determined TPP activity from *P. americana* at 32°C. These results indicate that TPP exhibits a wide variation in optimum temperature profiles.

Enzyme activity was tested at different T6P substrate concentrations (Figure 4). Increasing the substrate concentration only increases the reaction velocity up to the T6P concentration that produces the maximum TPP catalytic capacity (maximal velocity).

The substrate concentration curve (T6P [mM]) versus the initial velocity (V_0) is shaped as the perfect rectangular hyperbola (Figure 4) described by the Henri-Michaelis-Menten equation (Segel, 1979). At low substrate concentrations, the initial reaction velocity was approximately proportional to the T6P concentration, indicating the first order kinetic region. As the concentration of the substrate increases, the initial velocity of the reaction is no longer proportional to the concentration of the substrate.

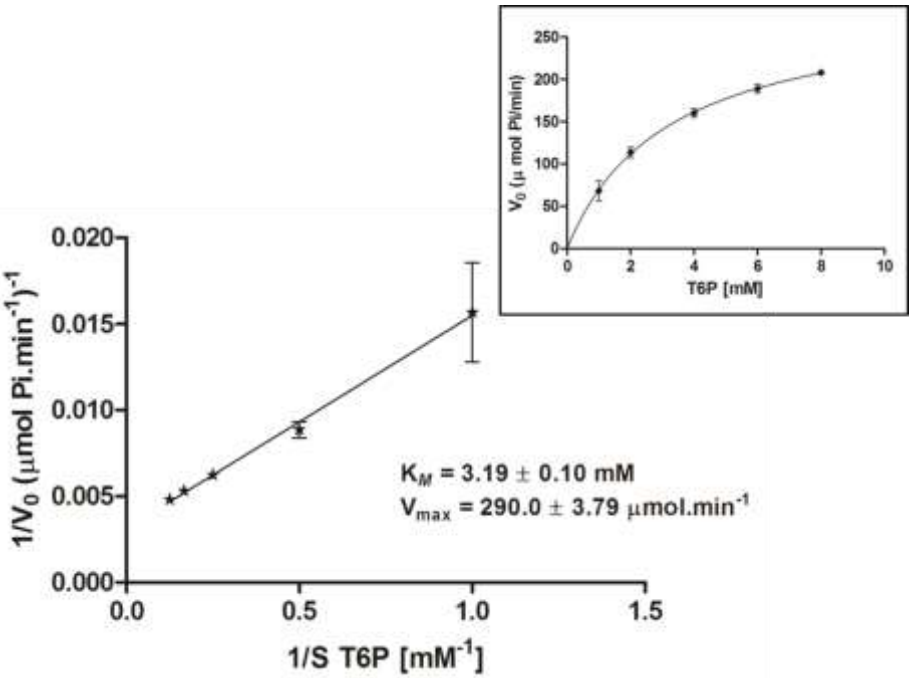

Figure 4. Kinetic constants of recombinant TPP from *A. gambiae*. K_M and V*max* were determined in triplicate using non-linear regression. The Michaelis-Menten curve was obtained with substrate concentrations between 1 - 8 mM and is presented at the right upper corner. The Lineweaver-Burk plot is highlighted.

The substrate concentration necessary to reach half-maximal velocity (½ *Vmax*) corresponds to K_M, the Michaelis-Menten constant (Figure 4) (Campbell and Farrell, 2007). The K_M value is important for the characterization of enzyme kinetics because different enzymes may have the same maximal initial velocity but generally will not have the same K_M, which indicates the difference in the amount of substrate required to saturate the enzyme (Vieira, 2003).

The recombinant TPP *Vmax* was 290.0 ± 3.79 µmol.min^{-1}, and K_M was 3.19 ± 0.10 mM, which is on the same order of magnitude of most of the reported TPPs: 2.5 ± 0.1 mM (Seo et al., 2000), 1.5 mM (Silva et al., 2005), 6.1 ± 1.5 mM (Nobre et al., 2008), 0.42 mM (Kushwaha et al., 2011), 0.39 ± 0.16 mM (Li et al., 2012), 0.36 ± 0.06 mM (Farelli et al., 2014), 0.87± 0.06 mM (Miao et al., 2016), 0.48 mM (Shan et al. 2016), 0.23 ± 0.07, 0.50 ± 0.10, 0.69 ± 0.07 and 0.31 ± 0.04 mM (Liu et al., 2017a).

Inhibition tests were performed to search for organic or inorganic chemical inhibitors of the recombinant TPP. The results of chemical inhibition tests on TPP activity at inhibitor concentrations of 5 and 25 mM are presented in Figure 5.

All of the tested chemical compounds inhibited TPP activity at 25 mM. At 5 mM, only two of the tested compounds ($CaCl_2$ and $Ca(NO_3)_2$) significantly inhibited TPP activity (Figure 5).

An ANOVA with Bonferroni correction performed on the results presented in Figure 5 confirmed that all of the chemical inhibitors tested at 25 mM resulted in significant inhibition (p<0.001; <0.0001) compared with that of the control, indicating that these compounds effectively inhibited TPP activity at this concentration. However, only two of the tested compounds at 5 mM ($CaCl_2$ and $Ca(NO_3)_2$) effectively inhibited recombinant TPP (p<0.001 and p<0.05, respectively).

These results indicate that compounds containing the Ca^{2+} divalent cation more effectively inhibit TPP, which is a result of the ion competing with Mg^{2+} for the enzyme active site, particularly for the substrate phosphate group, which characterizes competitive inhibition. Compounds containing Ca^{2+} ions have an inhibiting effect on phosphatases (Mamedov et al., 2001; Peeraer et al., 2004).

EDTA and NaF are considered non-competitive inhibitors because their inhibition depends on the concentration of these compounds but no concentrations of substrate or cofactor (Matula et al., 1971).

EDTA was reported to inhibit TPP from the bacteria *Mycobacterium smegmatis* (Matula et al., 1971) and the nematode *Brugia malayi* (Kushwaha et al., 2011). EDTA inhibition is caused by its action as a chelating agent because it forms stable complexes with several metal ions, including Mg^{2+} (the TPP cofactor) at pH values higher than 7 (Holleman and Wiberg, 2001). EDTA

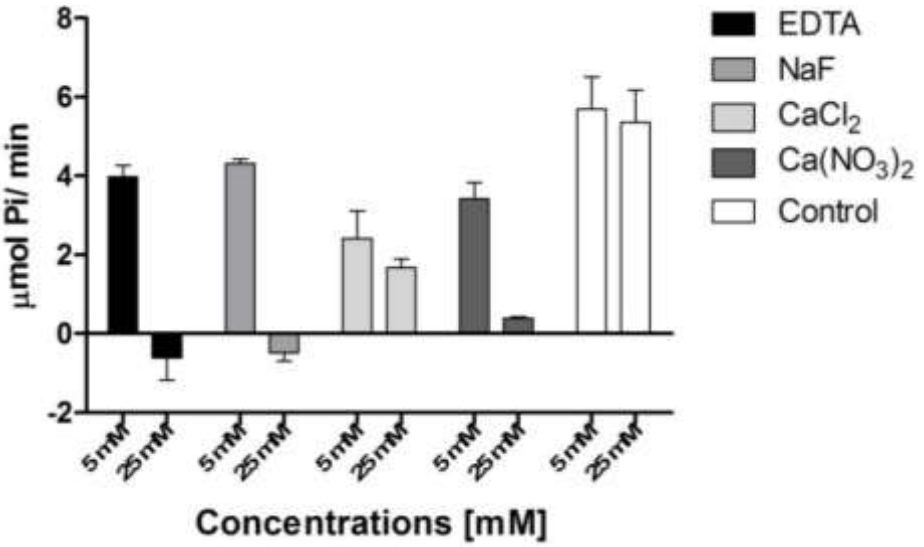

Figure 5. Effect of chemical inhibitors at 5 and 25 mM on recombinant TPP activity.

treatment of TPP from *T. acidophilum* resulted in the loss of its activity, suggesting that TPP is Mg^{2+} dependent (Rao et al., 2006). EDTA may therefore render the enzyme non-functional.

However, the inhibitory effect of NaF is caused by its action as a non-competitive phosphatase inhibitor (Matula et al., 1971). Friedman (1966) also observed that NaF inhibited TPP produced by *P. regina* by 70% when applied at 25 mM, which is the same concentration that inactivated recombinant TPP in the present study.

A standard BLASTP search at the UniProtKB web server identified several protein sequences with significant similarity to TPP from *A. gambiae*. The best hits were TPP from vector mosquitoes such as *Anopheles darlingi* (W5JSV8_ANODA), *Anopheles aquasalis* (T1E9M2_ANOAQ), *Culex quinquefasciatus* (B0WQL2_CULQU), *Aedes albopictus* (A0A023EMC7_AEDAL) and *Aedes aegypti* (Q16S69_AEDAE). The *A. gambiae* native enzyme (Q7PJ67_ANOGA) sequence was also considered in this search for comparison purposes. In the BLAST analysis, the trehalose phosphatase amino acid sequence showed 89% similarity to the TPP from *A. darlingi*, 88% similarity to *A. aquasalis*, 72% similarity to *C. quinquefasciatus*, 67% similarity to *A. albopictus* and 65% similarity to *A. aegypti*. These mosquitoes are important vectors of diseases transmitted by parasites and viruses, with *A. darlingi* the main vector of malaria in Neotropical regions, *A. aquasalis* a malaria vector in coastal areas of South and Central America, *C. quinquefasciatus* a vector for bancroftian filariasis, Oropouche virus and Nile fever, *A. albopictus* a vector for chikungunya virus and dengue and *A. aegypti* a vector for yellow fever, chikungunya, dengue and zyka. The sequences of TPP from *A. gambiae* and the remaining vector mosquitoes were subjected to multiple alignments using Clustal Omega from the European Molecular Biology Laboratory - European Bioinformatics Institute (EMBL-EBI) site (Figure 6).

TPP contains highly conserved motifs that are characteristic of the HAD superfamily (Figure 6). The motif I sequence has the DxD signature. The carboxylate group of the first aspartate (Asp) and carboxyl radical of the second Asp coordinate the cofactor Mg^{2+}. In addition, the first Asp of motif I acts as a nucleophile and forms an aspartyl intermediate during catalysis (Baker et al., 1998; Collet et al., 1997; Morais et al., 2000). Motif II is characterized by a highly conserved threonine or serine amino acid (Burroughs et al., 2006). Motif III is centered on a conserved lysine that occurs around the N-terminal portion of the α-helix region. Motifs II and III contribute to the stability of hydrolysis intermediaries. Motif IV is characterized by a conserved acidic residues. The acidic residues of motif IV typically exhibit one of three signatures: DD, GDxxxD or GDxxxxD (where x is any amino acid). For TPP from *A. gambiae*, the signature of motif IV is represented by GDxxxD acidic residues. Motifs I-IV are spatially arranged around the binding cleft at the end of the C-terminal region of the central sheet strands that form the active site of the HAD superfamily (Burroughs et al., 2006).

The multiple sequence alignment using Clustal Omega showed high similarity between TPP from different vector insects. However, the amino acids from vector insect proteins exhibited low similarity with the 1U02 template sequence; the amino acid composition of the motif regions from the template sequence and vector mosquitoes were similar. The catalytic site residues of TPP from *T. acidophilum* (1U02) have also been found in insect TPP. The only disparities were the residues of

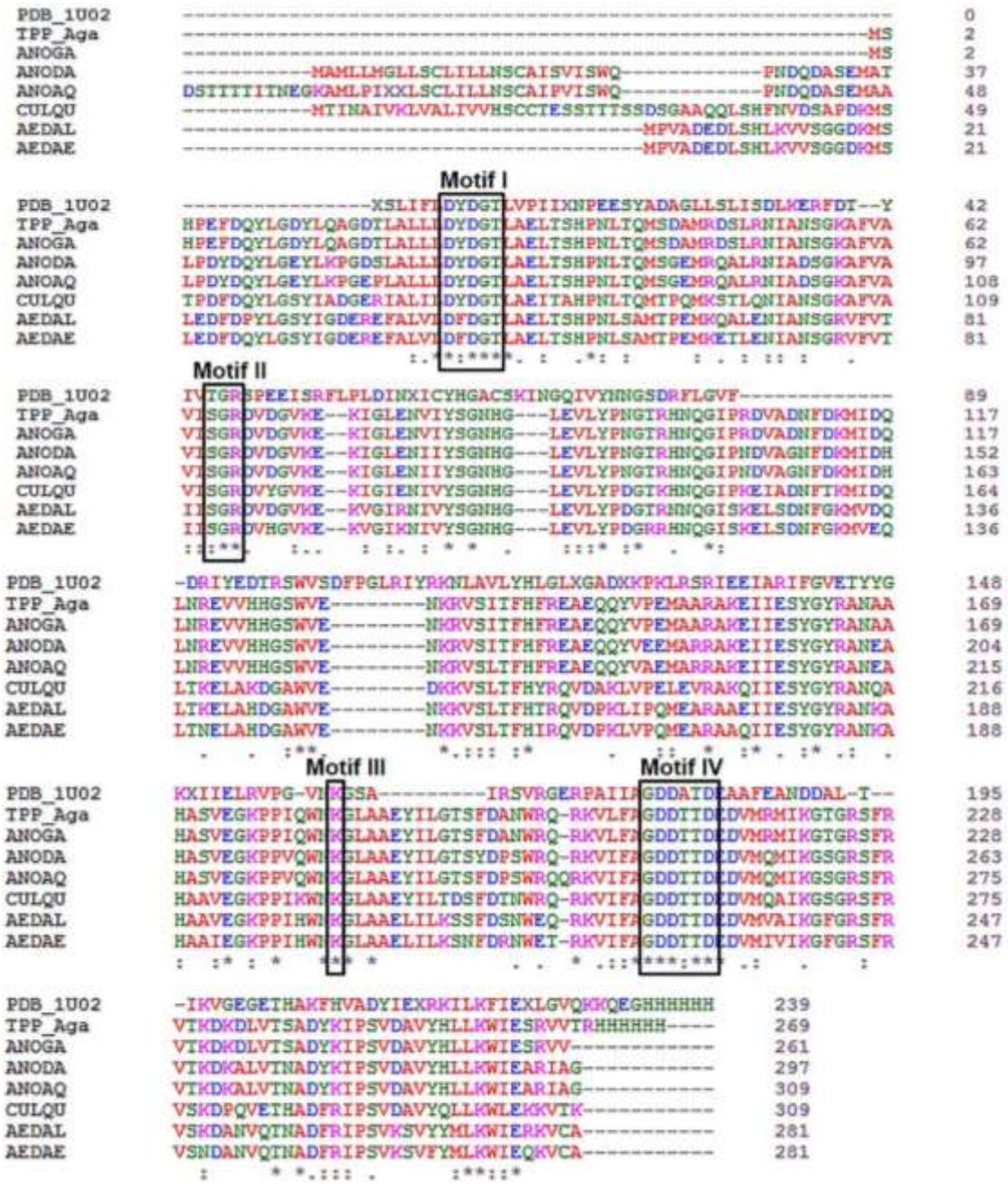

Figure 6. Alignment of the amino acid sequences of recombinant TPP with TPP sequences from different species of vector mosquitoes compared with that of the *T. acidophilum* template sequence. Identification of TPP sequences: PDB_1U02 (TPP from *T. acidophilum*), TPP_Aga (TPP from *A. gambiae* produced by *P. pastoris*), ANOGA (native TTP from *A. gambiae*), ANODA (from *Anopheles darlingi*), ANOAQ (from *Anopheles aquasalis*), CULQU (from *Culex quinquefasciatus*), AEDAL (from *Aedes albopictus*), AEDAE (from *Aedes aegypti*). Meaning of symbols under the sequences: ***** - identical regions; :- conserved regions; .- semiconserved regions. Regions with black rectangles indicate conserved motifs of the HAD superfamily: motif I - DXXX(T/V); motif II - (S/T)GX; motif III - K, motif IV - (G/S)(D/S)XXX(D/N).

motif II, where TPP from *T. acidophilum* has a threonine and insect TPP has a serine. In addition, the presence of a histidine tail at the TPP C-terminal portion does not appear to affect its biological function because it is distant from the functional motifs containing the catalytic residues.

One significant observation was the presence of a possible C2-type cap (Figure 7B). This cap is composed

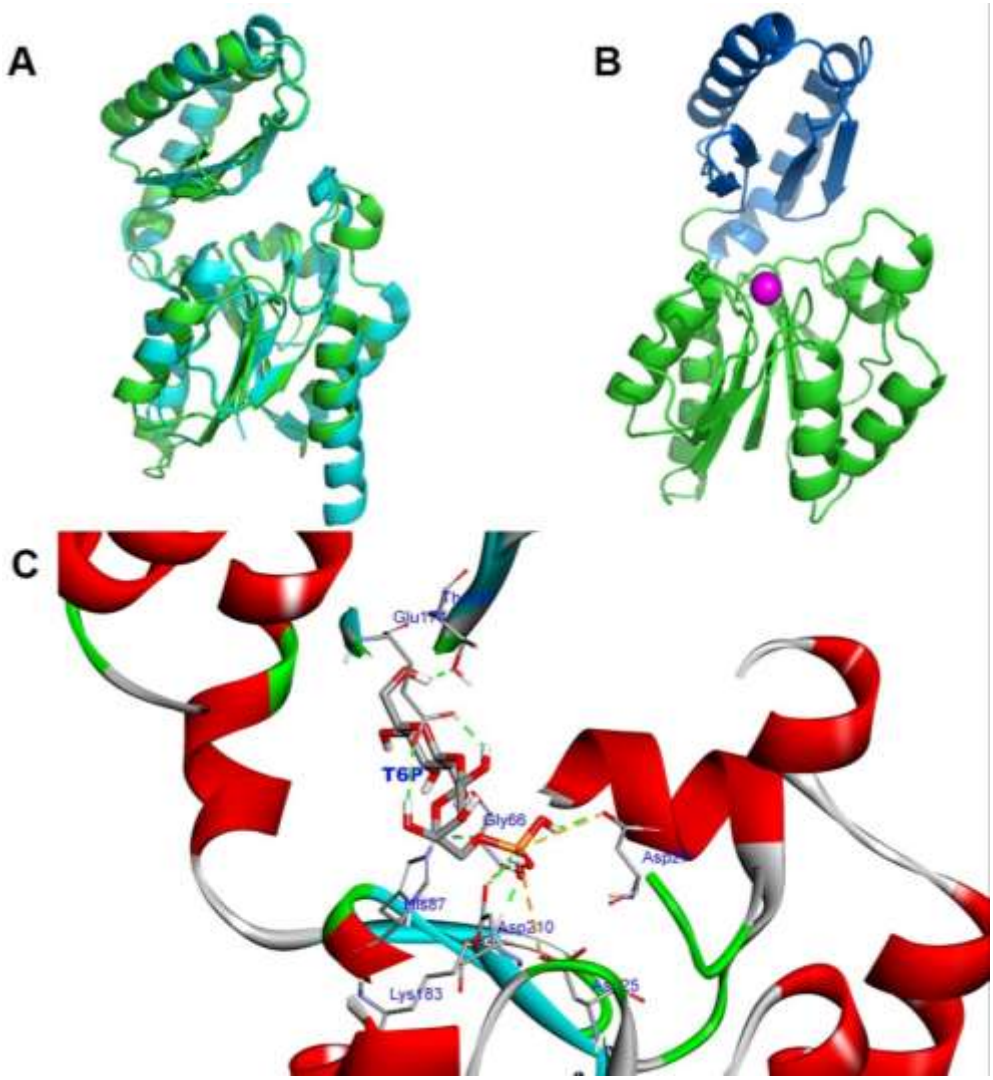

Figure 7. Structures of TPP from *A. gambiae* with their homologous model and simulation docking. **(A)** Ribbon diagram of the alignment of structural models for TPP from *A. gambiae* (green) and *T. acidophilum* (blue). The aligned structures were highly consistent between the two models. **(B)** Ribbon diagram of the tridimensional structure of TPP from *A. gambiae*, with the HAD central domain in green and the C2 cap domain in blue. Cofactor $Mg^{2+}$is indicated in magenta. **(C)** Simulation of T6P docking at the active site of TPP from *A. gambiae*. The T6P molecule represented in the line model is fit into the pocket formed between the central and cap domains. A detailed view of the active site shows the conserved residues involved in substrate binding. Green lines represent hydrogen bonds, and orange lines represent electrostatic interactions. Figure 7C was generated using the software AutoDock 4.2 and manipulated using the Discovery Studio 4.0 Visualizer.

of two consecutive units containing an α-helix followed by two β-strands (Figure 7B). The presence of this modification characterize a large clade within the HAD superfamily, which includes TPP and other phosphatases (Burroughs et al., 2006).

The tridimensional structure of recombinant TPP was obtained using the Phyre[2] web server. The stereochemical and general structural quality of the model generated by Phyre[2] was evaluated through an analysis of the Ramachandran plot using ProCheck, which showed that 92.9% of the residues estimated by the model were in the most favorable regions, 6.2% were in allowed regions, and 0.9% was in disallowed regions. Following validation, the tridimensional structure of TPP from *A. gambiae* was refined using the software ModRefiner and aligned with template 1U02 using the software PyMOL. The alignment of the two structural models is presented in Figure 7A.

The structural model exhibited 83% alignment coverage of the template 1U02, for which 223 amino acid residues were modeled with 100% confidence (probability that the *A. gambiae* sequences and template were homologues). The constructed model was based on an alignment generated using the Hidden Markov Model (HMM) maximum discrimination method (Eddy et al., 1995). The alignment quality was evaluated using the template modeling score, or TM-score (Zhang and Skolnick, 2005), which is a measure of structural similarity between two protein structures. The alignment of the structural model generated for *A. gambiae* TPP with the template revealed that the two models were consistent and indicated high reliability of the predicted structure for *A. gambiae* TPP.

The caps often contribute with residues that are required for specificity or auxiliary catalytic functions, and they play a central role in reactions catalyzed by the majority of HAD enzymes (Kurihara et al., 1995; Olsen et al., 1988). During the catalytic cycle, the cap domain moves across the catalytic site through binding interactions with the substrate-leaving group and forms a highly encapsulated active site (Farelli et al., 2014; Miao et al., 2016; Liu et al., 2017b). TPP typically has C2-type cap domains (in blue in Figure 7B) that project outward from the central domain (in green in Figure 7B). This type of domain is typical of the trehalose phosphatase family (Burroughs et al., 2006).

T6P binding to the TPP active site was modeled using the software AutoDock with a PyRx graphic interface (Figure 7C). The results were analyzed following protein visualization using Discovery Studio. Relevant information was obtained for the orientation of the enzyme-substrate binding interactions using AutoDock. For the docking simulations, the best binding position was the most energetically favorable one. The lowest binding free energy (ΔG_b) found for complex TPP-T6P was -4.30 kcal/mol, and the substrate molecule was stretched and interacted with the catalytic residues of the active site as expected. Therefore, the substrate fit well into the catalytic pocket formed at the interface of the central and cap domains near the active site residues. The substrate specificity for phosphatase is known to be dictated by the interface surface between these two domains (Farelli et al., 2014; Rao et al., 2006).

The interactions of T6P with TPP residues are presented in Figure 7C. The T6P sugar group is located at the cleft opening between the two domains, and it establishes hydrogen bonds with residues His87, Thr137 and Glu174, indicating that these residues may be involved in T6P binding. However, the phosphate group is located inside of the enzyme active site, where it can interact with catalytic residues Asp25, Asp27, Gly66, Lys183 and Asp210. The results obtained using AutoDock are consistent with the description of the main residues involved in interactions with the substrate. The interaction of the phosphate group with the catalytic residues of the active site is observed through hydrogen bonds, which are represented as dashed green lines, between the substrate oxygen (red tips of the phosphate group) and residues belonging to the HAD superfamily conserved motifs Asp27 (motif I), Gly66 (motif II), Lys183 (motif III) and Asp210 (motif IV). Electrostatic interactions (dashed orange lines) may occur between the substrate phosphorus and Asp residue (Asp25, Asp27 and Asp210) oxygen. The structure of the complex formed between the ligand and macromolecule supplies important information on the interactions that may occur at the active site, including hydrophobic and electrostatic interactions, hydrogen bonds and others. Figure 7C presents a detailed view of the catalytic site of TPP from *A. gambiae* and shows the evolutionary conservation of its component amino acids compared with the site of TPP from *T. acidophilum*. In addition, the similarity in spatial organization of the residues between the two enzymes was evident, indicating an affinity for the same type of substrate. Consequently, this pattern of T6P binding specificity is observed in other organisms that exhibit the trehalose biosynthesis pathway.

Because trehalose is an important carbohydrate for the metabolism of insects, studies have focused on the enzymes of its biosynthetic pathway to determine potential inhibitors. Kern et al. (2012) suggested that interference in trehalose synthesis could lead to the discovery of new insecticide action mechanisms because TPS (the other enzyme involved in trehalose synthesis) is also a potential drug target. The mechanism of inhibition of trehalose synthesis enzymes as a viable contribution to new insecticides is supported by previous studies (Chen et al., 2010; Tang et al., 2010). Trehalose was suggested as a likely source of energy for *Plasmodium* in *A. gambiae* mosquitoes after they feed on blood infected with these pathogens, since the parasite directly captures and metabolizes trehalose or is hydrolyzed to glucose and then captured by *Plasmodium* (Liu et al., 2013).

Recently, important drug target candidates were identified in the *B. malayi* nematode, that cause human filariasis, and TPP was one of the most important selected targets (Farelli et al., 2014). A vaccine is currently being developed using recombinant TPP from *B. malayi* with the goal of decreasing or preventing the development of the lymphatic filariasis parasite, and it has shown promising preliminary results (Kushwaha et al., 2013). Therefore, TPP is a key enzyme that plays a fundamental role in insect metabolism and physiology, and its absence in mammalian cells makes it a target for insecticide development.

Conclusions

The results of the present study show that the *P. pastoris* expression system provided efficient and stable source of TPP from *A. gambiae*. The purified recombinant enzyme presented good activity for its specific substrate.

Homology modeling confirmed that TPP is a monomer and has a similar structure to the enzyme's crystallography deposited at the data bank, conserving the catalytic motifs of the active site.

As the trehalose metabolism is essential for insects and in this work several structural and kinetic aspects were elucidated for the first time of one of the important enzymes involved in this metabolic pathway from *A. gambiae*, the results increase the knowledge of the biochemistry and biology of this mosquito, that is the main vector of malaria on the African continent.

Based on the present study, it will also be possible to screen for new inhibitors assaying directly drugs or extracts against TPP or using its 3D modeled structure to do virtual screening by docking, and this can be the basis for the development of new insecticides to control mosquito vectors of important diseases.

CONFLICT OF INTERESTS

The authors have not declared any conflict of interests.

ACKNOWLEDGEMENTS

The authors wish to thank Dr. Luís André Morais Mariúba from the Leonidas and Maria Deane Research Institute from the Oswaldo Cruz Foundation - Amazon (ILMD-Fiocruz/AM) for their help with the immunoassay tests. This study was financed by the National Council for Scientific and Technological Development (CNPq), Coordination for the Improvement of Higher Education Personnel (CAPES) and the Amazon Research Support Foundation (FAPEAM).

REFERENCES

Accelrys Software (2013). Discovery studio modeling environment. Release 4.0 Accelrys Software Inc. San Diego.

Baker AS, Ciocci MJ, Metcalf WW, Kim J, Babbitt PC, Wanner BL, Martin BM, Dunaway-Mariano D (1998). Insights into the mechanism of catalysis by the P-C bond-cleaving enzyme phosphonoacetaldehyde hydrolase derived from gene sequence analysis and mutagenesis. Biochemistry 37(26):9305-9315.

Behm CA (1997). The role of trehalose in the physiology of nematodes, Int. J. Parasitol. 27(2):215-229.

Bolton EE, Wang Y, Thiessen PA, Bryant SH (2008). PubChem: integrated platform of small molecules and biological activities. In. Wheeler R, Spellmeyer D, editors. Annual Reports in Computational Chemistry. American Chemical Society: Washington. Pp. 217-241.

Burroughs AM, Allen KN, Dunaway-Mariano D, Aravind L (2006). Evolutionary genomics of the HAD superfamily: understanding the structural adaptations and catalytic diversity in a superfamily of phosphoesterases and allied enzymes. J. Mol. Biol. 361(5):1003-1034.

Cabib E, Leloir LF (1958). The biosynthesis of trehalose phosphate. J. Biol. Chem. 231(1):259-275.

Campbell MK, Farrell SO (2007). Bioquímica. Thomson Editora.

Cereghino JL, Cregg JM (2000). Heterologous protein expression in the methylotrophic yeast *Pichia pastoris*. FEMS Microbiol. Rev. 24(1):45-66.

Chen J, Zhang D, Yao Q, Zhang J, Dong X, Tian H, Chen J, Zhang W (2010). Feeding-based RNA interference of a trehalose phosphate synthase gene in the brown planthopper, *Nilaparvata lugens*. Insect Mol. Biol. 19(6):777-786.

Collet JF, Gerin I, Rider MH, Veiga-da-Cunha M, van Schaftingen E (1997). Human L-3-phosphoserine phosphatase: sequence, expression and evidence for a phosphoenzyme intermediate. FEBS Lett. 408(3):281-284.

Collet JF, Stroobant V, Pirard M, Delpierre G, van Schaftingen E (1998). A new class of phosphotransferases phosphorylated on an aspartate residue in an amino-terminal DXDX(T/V) motif. J. Biol. Chem. 273(23):14107-14112.

Cregg JM, Tolstorukov I, Kusari A, Sunga J, Madden K, Chappell T (2009). Expression in the yeast *Pichia pastoris*. Methods Enzymol. 463:169-188.

DeLano WL (2006). An Executable PyMOL Incentive Product Based on PyMOL v0.99. Delano Scientific LLC: South San Francisco.

Eastmond PJ, van Dijken AJ, Spielman M, Kerr A, Tissier AF, Dickinson HG, Jones JD, Smeekens SC, Graham IA (2002). Trehalose-6-phosphate synthase 1, which catalyses the first step in trehalose synthesis, is essential for *Arabidopsis* embryo maturation. Plant J. 29(2):225-235.

Edavana VK, Pastuszak I, Carroll JD, Thampi P, Abraham EC, Elbein AD (2004). Cloning and expression of the trehalose-phosphate phosphatase of *Mycobacterium tuberculosis*: comparison to the enzyme from *Mycobacterium smegmatis*. Arch. Biochem. Biophys. 426(2):250-257.

Eddy SR, Mitchison G, Durbin R (1995). Maximum discrimination hidden Markov models of sequence consensus. J. Comput. Biol. 2(1):9-23.

Elbein AD (2009). Cytoplasmic carbohydrate molecules: trehalose and glycogen. In. Moran AP, Holst O, Brennan P, von Itzstein M, editors. Microbial Glycobiology: Structures, Relevance and Applications. Academic Press: London. P. 1020.

Elbein AD, Pan YT, Pastuszak I, Carroll D (2003). New insights on trehalose: a multifunctional molecule. Glycobiology 13(4):17R-27R.

Farelli JD, Galvin BD, Li Z, Liu C, Aono M, Garland M, Hallett OE, Causey TB, Ali-Reynolds A, Saltzberg DJ, Carlow CK, Dunaway-Mariano D, Allen KN (2014). Structure of the trehalose-6-phosphate phosphatase from *Brugia malayi* reveals key design principles for anthelmintic drugs. PLOS Pathog. 10(7):e1004245.

Forattini OP (2002). Culicidologia médica: Identificação, Biologia e Epidemiologia. 2nd vol. USP: São Paulo.

Friedman S (1966). Trehalose-6-phosphate phosphatase from insects. Methods Enzymol. 8:372-374.

Friedman S, Hsueh T (1979). Insect trehalose-6-phosphatase: the unactivated type, as illustrated in *Periplaneta americana*, and a survey of the ordinal distribution of the two presently known types. Comp. Biochem. Physiol. 64B(4):339-344.

Garcia LS (2010). Malaria. Clin. Lab. Med. 30(1):93-129.

Gravel P (2002). Protein blotting by the semidry method. In. Walker JM, editor. The Protein Protocols Handbook. Humana Press: Totowa. Pp. 321-334.

Holleman AF, Wiberg E (2001). Inorganic Chemistry. Academic Press: Zurich, Switzerland.

Karthik L, Malathy P, Trinitta A, Gunasekaran K (2011). Molecular docking with trehalose-6 phosphate phosphatase: A potential drug target of filarial parasite "*Brugia malayi*". Lett. Drug Des. Discov. 8(4):363-370.

Kelley LA, Sternberg MJ (2009). Protein structure prediction on the web: a case study using the Phyre server. Nat. Protoc. 4(3):363-371.

Kern C, Wolf C, Bender F, Berger M, Noack S, Schmalz S, Ilq T (2012). Trehalose-6-phosphate synthase from the cat flea *Ctenocephalides felis* and *Drosophila melanogaster*: gene identification, cloning, heterologous functional expression and identification of inhibitors by high throughput screening. Insect Mol. Biol. 21(4):456-471.

Klowden MJ (2013). Physiological Systems in Insects. 3rd ed. Academy Press: Moscow.

Klutts S, Pastuszak I, Edavana VK, Thampi P, Pan YT, Abraham EC, Carroll JD, Elbein AD (2003). Purification, cloning, expression, and properties of mycobacterial trehalose-phosphate phosphatase. J. Biol. Chem. 278(4):2093-2100.

Koonin EV, Tatusov RL (1994). Computer analysis of bacterial haloacid dehalogenases defines a large superfamily of hydrolases with diverse specificity. Application of an iterative approach to database search. J. Mol. Biol. 244(1):125-132.

Kormish JD, McGhee JD (2005). The *C. elegans* lethal gut-obstructed *gob-1* gene is trehalose-6-phosphate phosphatase. Dev. Biol. 287(1):35-47.

Kurihara T, Liu JQ, Nardi-Dei V, Koshikawa H, Esaki N, Soda K (1995). Comprehensive site-directed mutagenesis of L-2-halo acid dehalogenase to probe catalytic amino acid residues. J. Biochem. 117(6):1317-1322.

Kushwaha S, Singh PK, Rana AK, Misra-Bhattacharya S (2011).Cloning, expression, purification and kinetics of trehalose-6-phosphate phosphatase of filarial parasite *Brugia malayi*. Acta Trop. 119(2-3):151-159.

Kushwaha S, Singh PK, Rana AK, Misra-Bhattacharya S (2013). Immunization of *Mastomys coucha* with *Brugia malayi* recombinant trehalose-6-phosphate phosphatase results in significant protection against homologous challenge infection. PLOS One 8(8):e72585.

Laemmli UK (1970).Cleavage of structural proteins during the assembly of the head of bacteriophage T4. Nature 227(5259):680-685.

Laskowski RA, MacArthur MW, Moss DS, Thornton JM (1993). Procheck: A program to check the stereochemical quality for assessing the accuracy of protein structures. J. Appl. Crystallogr. 26(2):283-291.

Li YT, Zhang HH, Sheng HM, An LZ (2012). Cloning, expression and characterization of trehalose-6-phosphate phosphatase from a psychotropic bacterium, *Arthrobacter* strain A3. World J. Microbiol. Biotechnol. 28(8):2713-2721.

Liu C, Dunaway-Mariano D, Mariano PS (2017a). Rational design of first generation inhibitors for trehalose 6-phosphate phosphatases. Tetrahedron 73(10):1324-1330.

Liu C, Dunaway-Mariano D, Mariano PS (2017b). Rational design of reversible inhibitors for trehalose 6-phosphate phosphatases. Eur. J. Med. Chem. 128:274-286.

Liu K, Dong Y, Huang Y, Rasgon JL, Agre P (2013). Impact of trehalose transporter knockdown on *Anopheles gambiae* stress adaptation and susceptibility to *Plasmodium falciparum* infection. Proc. Natl. Acad. Sci. 110(43):17504-17509.

Mamedov TG, Suzuki K, Miura K, Kucho Ki K, Fukuzawa H (2001). Characteristics and sequence of phosphoglycolate phosphatase from a eukaryotic green alga *Chlamydomonas reinhardtii*. J. Biol. Chem. 276(49):45573-45579.

Matula M, Mitchell M, Elbein AD (1971). Partial purification and properties of a highly specific trehalose phosphate phosphatase from *Mycobacterium smegmatis*. J. Bacteriol. 107(1):217-222.

Miao Y, Tenor JL, Toffaletti DL, Washington EJ, Liu J, Shadrick WR, Schumacher MA, Lee RE, Perfect JR, Brennan RG (2016). Structures of trehalose-6-phosphate phosphatase from pathogenic fungi reveal the mechanisms of substrate recognition and catalysis. Proc. Natl. Acad. Sci. USA. 113(26):7148-7153.

Morais MC, Zhang W, Baker AS, Zhang G, Dunaway-Mariano D, Allen KN (2000). The crystal structure of *Bacillus cereus* phosphonoacetaldehyde hydrolase: insight into catalysis of phosphorus bond cleavage and catalytic diversification within the HAD enzyme superfamily. Biochemistry 39(34):10385-10396.

Morris GM, Goodsell DS, Halliday RS, Huey R, Hart WE, Belew RK, Olson AJ (1998). Automated docking using a Lamarckian genetic algorithm and an empirical binding free energy function. J. Comput. Chem. 19(14):1639-1662.

Nobre A, Alarico S, Fernandes C, Empadinhas N, da Costa MS (2008). A unique combination of genetic systems for the synthesis of trehalose in *Rubrobacter xylanophilus*: properties of a rare actinobacterial TreT. J. Bacteriol. 190(24):7939-7946.

Oakley BR, Kirsch DR, Morris NR (1980). A simplified ultrasensitive silver stain for detecting proteins in polyacrylamide gels. Anal. Biochem. 105(1):361-363.

Olsen DB, Hepburn TW, Moos M, Mariano PS, Dunaway-Mariano D (1988). Investigation of the *Bacillus cereus* phosphonoacetaldehyde hydrolase. Evidence for a Schiff base mechanism and sequence analysis of an active-site peptide containing the catalytic lysine residue. Biochemistry 27(6):2229-2234.

Peeraer Y, Rabijns A, Collet JF, van Schaftingen E, de Ranter C (2004).How calcium inhibits the magnesium-dependent enzyme human phosphoserine phosphatase. Eur. J. Biochem. 271(16):3421-3427.

Rao KN, Kumaran D, Seetharaman J, Bonanno JB, Burley SK, Swaminathan S (2006). Crystal structure of trehalose-6-phosphate phosphatase-related protein: biochemical and biological implications. Protein Sci. 15(7): 1735-1744.

Segel IH (1979). Bioquímica: teoria e problemas. Livros Técnicos e Científicos Editora: Rio de Janeiro.

Seo HS, Koo YJ, Lim JY, Song JT, Kim CH, Kim JK, Lee JS, Choi YD (2000). Characterization of a bifunctional enzyme fusion of trehalose-6-phosphate synthetase and trehalose-6-phosphate phosphatase of *Escherichia coli*. Appl. Environ. Microbiol. 66(6):2484-2490.

Shan S, Min H, Liu T, Jiang D, Rao Z (2016). Structural insight into dephosphorylation by trehalose 6-phosphate phosphatase (OtsB2) from *Mycobacterium tuberculosis*. FASEB J. 30(12):3989-3996.

Sievers F, Wilm A, Dineen D, Gibson TJ, Karplus K, Li W, Lopez R, McWilliam H, Remmert M, Söding J, Thompson JD, Higgins DG (2011). Fast, scalable generation of high-quality protein multiple sequence alignments using Clustal Omega. Mol. Syst. Biol. 7(1):539.

Silva Z, Alarico S, da Costa MS (2005). Trehalose biosynthesis in *Thermus thermophilus* RQ-1: biochemical properties of the trehalose-6-phosphate synthase and trehalose-6-phosphate phosphatase. Extremophiles 9(1):29-36.

Solis FJ, Wets RJ (1981). Minimization by random search techniques. Math. Oper. Res. 6(1):19-30.

Tang B, Chen J, Yao Q, Pan Z, Xu W, Wang S, Zhang W (2010).Characterization of a trehalose-6-phosphate synthase gene from *Spodoptera exigua* and its function identification through RNA interference. J. Insect Physiol. 56(7):813-821.

Tang B, Yang M, Shen Q, Xu Y, Wang H, Wang S (2017). Suppressing the activity of trehalase with validamycin disrupts the trehalose and chitin biosynthesis pathways in the rice brown planthopper, *Nilaparvata lugens*. Pest. Biochem. Physiol. 137:81-90.

Thompson SN (2003). Trehalose - the insect “blood” sugar. Adv. Insect Physiol. 31:205-285.

Vaidyanathan R, Estep A, Becnel J, Moore J, Talcott C (2015). Silencing trehalose-6-phosphate synthase incapacitates adult mosquitoes by interfering with the biosynthetic pathway for flight fuel. Mosquito and Fly Research. Agricultural Research Service: USDA.

Vieira R (2003). Fundamentos de bioquímica. UFPA: Belém.

Wolf LK (2009). PyRx. C&EN 87:31.

WHO (World Health Organization)(2016). World Malaria Report (2016). [http://www.who.int/malaria/publications/world-malaria-report-2016/report/en/].

Xu D, Zhang Y (2011). Improving the physical realism and structural accuracy of protein models by a two-step atomic-level energy minimization. Biophys. J. 101(10):2525-2534.

Zhang Y, Skolnick J (2005). TM-align: a protein structure alignment algorithm based on the TM-score. Nucleic Acids Res. 33(7):2302-2309.